RSC Advances

This is an *Accepted Manuscript*, which has been through the Royal Society of Chemistry peer review process and has been accepted for publication.

Accepted Manuscripts are published online shortly after acceptance, before technical editing, formatting and proof reading. Using this free service, authors can make their results available to the community, in citable form, before we publish the edited article. This *Accepted Manuscript* will be replaced by the edited, formatted and paginated article as soon as this is available.

You can find more information about *Accepted Manuscripts* in the Information for Authors.

Please note that technical editing may introduce minor changes to the text and/or graphics, which may alter content. The journal's standard Terms & Conditions and the Ethical guidelines still apply. In no event shall the Royal Society of Chemistry be held responsible for any errors or omissions in this *Accepted Manuscript* or any consequences arising from the use of any information it contains.

ROYAL SOCIETY OF CHEMISTRY

www.rsc.org/advances

Intriguing mechanical properties and its mechanism of highly enhanced compatibilization of two biopolymer blends

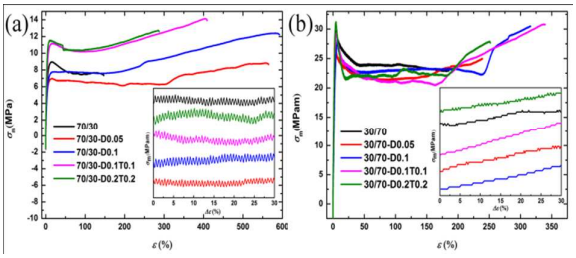

RSC Advances Accepted Manuscript

Cite this: DOI: 10.1039/c0xx00000x

www.rsc.org/xxxxxx

ARTICLE TYPE

Toughening mechanism behind intriguing stress-strain curves in tensile tests of highly enhanced compatibilization of biodegradable Poly(lactic acid)/Poly(3-hydroxybutyrate-*co*-4-hydroxybutyrate) blends

Yijie Bian[a, b], Changyu Han[a], Lijing Han[a], Haijuan Lin[a, b], Huiliang Zhang[a], Junjia Bian[a] and Lisong Dong*[a]

Received (in XXX, XXX) Xth XXXXXXXXX 20XX, Accepted Xth XXXXXXXXX 20XX
DOI: 10.1039/b000000x

Highly enhanced compatibilization of biosourced and biodegradable polylactide (PLA) and poly(3-hydroxybutyrate-*co*-4-hydroxybutyrate) (P(3HB-*co*-4HB)) blends were successfully prepared by reactive melt compounding. Large shifts toward each other of glass transition temperatures, a considerable reduction of the dispersed phase particle size and a significant increase of interfacial adhesion between the PLA and P(3HB-*co*-4HB) phases were observed after compatibilization. And the chain branches occurred during branching reaction decreased the crystallization ability of PLA, while crosslinks formed in crosslinking enhanced it on a large scale. Moreover, the blends exhibited remarkable improvement of rheological properties of melt state when compared with that of blank PLA/P(3HB-*co*-4HB) blends. With increasing the content of crosslinking agent dicumyl peroxide (DCP), the blends showed increased yield tensile strength, modulus, and elongation at break. However, when DCP cooperated with triallyl isocyanurate (TAIC), the elongation at break decreased because that crosslinking network limited the mobility of polymer chains to deform under tensile load. Most notably, two typical different kinds of growths of stress-strain curves were observed, and for the first time we demonstrated the toughening mechanism behind it in detail. Furthermore, SEM images of fracture surfaces of the blends reconfirmed it and that plastic deformation of matrix and debonding process were the two important ways induced energy dissipation and led to toughened blends.

Introduction

Polymer blends have received much attention due to combining attractive features of each component and reducing their deficient characteristics at the same time. The performance of polymer blends is determined not only by the property of each component but also by the morphology formed.[1-4] Actually, most of polymer blends are immiscible because of high interfacial tension and poor adhesion. However the mechanical properties of a multiphase system are usually driven by the ability of the interface to transmit stress from one phase to another.[5] Therefore, the compatibilization is vital necessary for immiscible polymer blends. This can be obtained by introducing a third component to refine the droplet size of dispersed minor phase, to lower the interfacial tension and stabilize it against coalescence, and to ensure strong interfacial adhesion between phases.[6] A considerable number of research works have been published on introducing nanoscale fillers or pre-made copolymers into polymer blends.[7-19] Compared with a third compatibilizer showing limited efficiency due to only relying on physical interaction, a free radical initiator, i.e., dicumyl peroxide (DCP), was introduced into the polylactide/poly(ε-caprolactone) blend and polylactide/poly(butylene succinate) blend to induce in situ compatibilization on a large scale.[20-22]

PLA has excellent high tensile strength and good biocompatibility, but also shows brittleness and difficulty in process. On the contrary, Poly(3-hydroxybutyrate-*co*-4-hydroxybutyrate) P(3HB-*co*-4HB) with high molar fraction of 4-hydroxybutyrate (4HB), is a promising bio-elastomer owning high flexibility in the big polyhydroxyalkanoates (PHAs) family.[23, 24] Biobased microbial PHAs, produced by *Ralstonia eutropha*, *Alcaligenes latus*, and *Comamonas acidovorans*,[25-27] have attracted universal attention due to their resources renewable, biodegradable properties, biocompatibility, and potential applications as environmental friendly polymers for agricultural, marine, and medical applications. Therefore, to blend PLA and P(3HB-*co*-4HB) becomes a reasonable choice to improve the flexibility and toughness of PLA for its many other potential applications. In order to enhance in-situ compatibilization, crosslinking is introduced additionally in the work by adding triallyl isocyanurate (TAIC) to cooperate with DCP. Since TAIC, used in industry as a common crosslinking

RSC Advances Accepted Manuscript

agent for polyolefin and vinyl polymers,[28] has also been reported to be an effective crosslinking agent for PLA due to double bonds in TAIC to improve the efficacy of free radicals.[29]

In this study, biodegradable and biosourced PLA/P(3HB-*co*-4HB) blends were prepared by melt compounding using crosslinking agents to enhance in-situ compatibilization. The aim of this work was to investigate different effects of branching and crosslinking on the morphology and compatibilization of the blends. Mostly importantly profound mechanical mechanism of the system was discussed in detail. Furthermore, the thermal and rheological properties of resultant blends were investigated.

Experimental

Materials

The PLA (Grade 4032D) used in this work was a commercially available product from Natureworks LLC (USA). It exhibited a weight-average molecular weight of 207kg/mol and polydispersity of 1.74 as determined by gel permeation chromatography (GPC). Bacterial copolymer P(3HB-*co*-4HB) was provided by Tianjin Guoyun Biotech (China). The number-average molecular weight was 195kg/mol with a polydispersity of 1.86 determined by GPC. The content of 4HB in the copolymer was 23.9 mol% determined by ^{1}H NMR spectroscopy. The free radical initiator DCP was purchased from Beijing Chemical Company (China). TAIC was purchased from Aldrich. All of these materials were used as received.

Blend preparation

Before processing, the two polymers were dried in a vacuum oven at 70 °C for 24 h. A certain amount of DCP and/or TAIC were/was dissolved precisely in acetone. Then the solution was mixed with two polymers and dried in a vacuum oven at 50 °C for another 12 h. After that the mixtures were mixed in an internal mixer (Rheomix 600p, Haake, Karlsruhe, Germany) at 165 °C and 50 rpm for 6 min. Then, the samples were hot-pressed at 185 °C for 3 min and then cold-pressed at room temperature to form sheets of 1 mm thick. The resultant samples were designated as *x*/*y*-D*a*/T*b*. Here *x* and *y* denote the weight percentage of PLA and P(3HB-*co*-4HB), *a* and *b* denote the weight percentage of DCP and TAIC, respectively. For comparison, neat PLA and neat P(3HB-*co*-4HB) were treated with the same procedure.

Characterizations

The gel content of the branched/crosslinked P(3HB-*co*-4HB) was determined gravimetrically with a Soxhlet extraction cycle with boiling chloroform as solvent for 24 h. Approximate 0.2 g samples were cut into small pieces and wrapped in a pre-weighted, quantitative filter paper. After the extraction, the extracted samples were vacuum-dried to a constant weight. The gel fraction was calculated as follows,

$$\text{Gel fraction} = (M_d/M_i) \times 100\% \quad (1)$$

where M_i is the initial weight of the sample and M_d is the dry weight of the sample after extraction.

Dynamic mechanical analysis (DMA) was carried out with a dynamic mechanical analyzer SDTA861^e (Melltler Toledo) in the tensile mode. The samples with gauge dimensions of 20×4×1mm^3 were used. The dynamic loss factor (tan δ) and the storage modulus (E') were determined at a frequency of 1 Hz and a heating rate of 3°C/min as a function of temperature from -60 to 120°C.

The phase morphology of the blends was investigated using a field emission scanning electron microscopy (XL30 ESEM FEG, FEI Co., Eindhoven, The Netherlands) at an accelerating voltage of 10 kV. The samples were immersed in liquid nitrogen for about 5 min, and then broken. Because of the similar physical properties of PLA and P(3HB-*co*-4HB) as aliphatic polyester, direct observation of the cryo-fractured surfaces of PLA/P(3HB-*co*-4HB) blends by SEM is difficult to obtain the obvious dispersed phase morphology. The selective enzymatic degradation method was used. For PLA matrix samples, remove the P(3HB-*co*-4HB) component from the cryo-fractured surfaces of the blends, and the remaining morphology was observed. The selective enzymatic degradation of the blends was carried out in phosphate buffer (pH 7.4) containing lipase from *Pseudomonas mendocina* at 37°C with shaking at 140 rpm. In addition, crosslinked P(3HB-*co*-4HB) with the gel fraction of about 40% had been treated with the same procedure to insure even crosslinked P(3HB-*co*-4HB) could be degraded by the lipase. (The lipase from *Pseudomonas mendocina* revealed that it prefers enzymatic degradation of P(3HB-*co*-4HB) but insignificant attacks to PLA in the blends.[30]) When the P(3HB-*co*-4HB) component on the surface of samples was degraded, the samples were removed , washed by distilled water, and dried to constant weight in vacuum. And for P(3HB-*co*-4HB) matrix samples, remove the PLA component from the cryo-fractured surfaces by using proteinase K with the same procedure.[31] Likely, crosslinked PLA with the gel fraction of about 40% had been treated with the same procedure to insure crosslinked PLA could be degraded by proteinase K. The degraded cryo-fractured surfaces of all the samples were sputter-coated with a thin layer of gold and observed with SEM.

Differential scanning calorimetry (DSC) experiments were carried out on a TA Instruments DSC Q20 (USA) under N_2 atmosphere. The specimens were sealed in aluminum crucibles and had a nominal weight of about 5±0.3 mg. The samples were heated from 40 °C to 185 °C at a heating rate of 30 °C /min (first heating), held for 2 min to erase previous thermal history, then cooled to 30 °C at a rate of 5 °C /min (first cooling). The samples were further heated to 185 °C again from 30 °C at a heating rate of 20 °C /min (second heating).

Rheological properties were measured by a rotational rheometer (TA Series AR2000ex, TA Instrument, USA). The compression-molded samples were cut into the disks with 25 mm in diameter and 1mm in thickness. The measurements were carried out in dynamic (oscillatory) mode by means of 25 mm parallel geometry at 180 °C under air atmosphere. Amplitude sweeps were performed in advance to ensure that dynamic tests were in the linear viscoelastic range and the strain value of 1.25% was consequently chosen. Frequency ranged from 0.1 to 100 rad/s.

Uniaxial tensile tests were carried out on dumbbell shaped specimens (20 × 4 × 1mm^3) who were punched out from the pressed sheets. The measurements were performed using a tensile-testing machine (Instron-1121) according to GB/T1040-

RSC Advances Accepted Manuscript

This journal is © The Royal Society of Chemistry [year]

2006 (China) at room temperature at a crosshead speed of 10 mm/min. At least five specimens were tested for each sample to get an average value.

Results and discussion

Gel analysis of the PLA/P(3HB-*co*-4HB) blends

Both PLA and P(3HB-*co*-4HB) can form branched and/or crosslinked structures with crosslinking agents as pure materials as shown in Figure 1. At the interface of the PLA/P(3HB-*co*-4HB) blends, branching/crosslinking can occur via a combination of PLA and P(3HB-*co*-4HB) free radicals. It has to be noted that the combination reaction of free radicals not only occurs at the interface, but can also occur in the PLA domains and P(3HB-*co*-4HB) domains. As a consequence, complex reaction products could be obtained, including branched/crosslinked PLA, branched/crosslinked P(3HB-*co*-4HB), PLA-*g*-P(3HB-*co*-4HB) copolymers, and PLA-crosslink-P(3HB-*co*-4HB) network. Furthermore, the melt blending was accompanied by chain scissions due to the thermal instability of both two kinds of polymers and the instability of free radicals, resulting in even more complicated products. Figure 1 shows the gel fraction of these blends. Obviously, there was no gel formed until the addition of TAIC as a co-crosslinking agent, and the gel fraction of the PLA/P(3HB-*co*-4HB) blends increased to near 40% by only adding 0.1wt% DCP and 0.1wt% TAIC. At certain amount of DCP, only branching and/or chain scissions reactions occurred, and from the later rheological properties measurements the complex viscosities of these blends were higher than that of blank blend, indicating branching reaction predominated over chain scissions. While as DCP cooperated with TAIC, crosslingking reaction became dominant. Additionally, TAIC proved to be an effective co-crosslinking agent in combination with DCP. It also can be learn that P(3HB-*co*-4HB) caused less chain scissions than that of PLA when existed with free radicals because of a relative higher gel fraction gained in crosslinked P(3HB-*co*-4HB) as adding the same amounts of crosslinking agents.

Figure 1

Miscibility and phase morphology

It is well known that when the two polymers are miscible in the amorphous phase they will show a single glass transition temperature (T_g), while appearance of two T_gs corresponding to each individual component which is the characteristic of immiscible blends. In partially miscible blends the T_gs of each component shifts toward each other. Figure 2(a,b) show tan δ vs. temperature for neat polymers and their blends. Each neat component exhibited a single relaxation peak corresponding to T_g. For all the blends, tan δ curves revealed two T_gs, the higher T_g was corresponding to PLA component, and the lower one was corresponding to P(3HB-*co*-4HB) component. Moreover, the T_gs of both PLA and P(3HB-*co*-4HB) components showed almost no shift toward each other in blank and branched blends, suggesting that PLA and P(3HB-*co*-4HB) were immiscible in these blends. However, one should notice that for crosslinked blends, owning to the formation of PLA-*g*-P(3HB-*co*-4HB) and PLA-crosslink-P(3HB-*co*-4HB) network, the T_gs of PLA and P(3HB-*co*-4HB) components showed large shifts toward each other, indicating an enhanced compatibilization. The crosslinked blends became partially miscible. Additionally, the difference of glass transition (ΔT_g) between PLA component and P(3HB-*co*-4HB) component in each blend was calculated in Table 1, 30/70 blends showed smaller ΔT_gs than those of 70/30 blends, indicating 30/70 blends achieved finer compatibility than that of 70/30 blends as adding the same contents of DCP and TAIC. As shown in Figure 2(c,d), the storage modulus (E') at room temperature for PLA/P(3HB-*co*-4HB) blends are above neat PLA and neat P(3HB-*co*-4HB), indicating both branching structure and crosslinking network can enhance chain entanglement. Additionally, the improvement of E's of 70/30 blends are a little lower than those of 30/70 blends. It was because PLA component suffered heavier thermal decomposition at the processing temperature than that of P(3HB-*co*-4HB) as mentioned above. In Figure 2(c), the E's of the blends dropped sharply about 0^{o}C due to the T_g of P(3HB-*co*-4HB), and then decreased again around 60 ^{o}C due to the T_g of PLA, but began to increase about 100 ^{o}C due to the cold crystallization of PLA. Moreover, the cold crystallization peak (T_{cc}) of PLA shifted to lower temperature (90 ^{o}C) for 70/30 blend and branched blends, and moved to 80 ^{o}C when crosslinking happened. These results suggested that the incorporation of both P(3HB-*co*-4HB) and crosslinking network enhanced the cold-crystallization ability of PLA and decreased the T_{cc} of PLA in the blends. In Figure 2(d), there was only a clear sharp drop around 0 ^{o}C owning to the T_g of P(3HB-*co*-4HB), and then an increase about 100 ^{o}C due to the cold crystallization of PLA and the same enhanced cold-crystallization of PLA were observed in 30/70 blends.

Figure 2

Figure 3 presents typical matrix-droplet morphology of cryo-fractured surfaces of PLA/P(3HB-*co*-4HB) blends after selective enzymatic degradation. The black pores were nicely appeared by the removal of dispersed phase on cryo-fractured surfaces of the blends. It was found that the blends displayed clear fine dispersion. In Figure 3(a,f), the particle sizes of these pores were very large and non-uniform. However in Figure 3(b-e, g-m), much finer and more uniform dispersion of the dispersive phase was obtained with the increasing of DCP and TAIC, attributing to in-situ formed PLA-*g*-P(3HB-*co*-4HB) copolymers and PLA-crosslink-P(3HB-*co*-4HB) network who acted as compatibilizer between PLA and P(3HB-*co*-4HB) domains. Moreover, crosslinked PLA and crosslinked P(3HB-*co*-4HB), all these reaction products not only decreased the viscosity ratio of two components but also increased the physical and chemical entanglement in the system, which prevented the coalescence of dispersed phase domains during melt mixing. So a large improvement of compatibility and strong interfacial adhesion between PLA and P(3HB-*co*-4HB) phases achieved. And much finer and more uniform dispersion was obtained in crosslinked blends than that of branched blends. What was more, 30/70 blends displayed more uniform and smaller average particle sizes of dispersed phase than those of 70/30 blends at the same amount of crosslinking agents, especially for 30/70-D0.05 vs. 70/30-D0.05 and for 30/70-D0.1 vs. 70/30-D0.1, which was in agreement with the results obtained from DMA measurements. To further explore the reason, the complex viscosities of neat PLA, P(3HB-*co*-4HB) and their blank blends are showed in Figure 4. At the given temperature (180^{o}C), the complex viscosity ($|\eta^*|$) of neat PLA is twice that of neat P(3HB-*co*-4HB),

RSC Advances Accepted Manuscript

and the $|\eta^*|$ of 70/30 blend is a little higher than that of 30/70 blend. Moreover, the lower viscous P(3HB-*co*-4HB) could be broken into smaller droplets and stabilized more easily than PLA. So more PLA-*g*-P(3HB-*co*-4HB) copolymers and/or PLA-crosslink-P(3HB-*co*-4HB) network occurred at the interface during reactive blending for 30/70 blends. Therefore, more uniform and smaller particle sizes were achieved in 30/70 blends.

Figure 3

Figure 4

Thermal Behavior

The DSC results of thermal behaviour for PLA/P(3HB-*co*-4HB) blends are shown in Figure 5 and parameters of thermal properties are listed in Table 1. Neat PLA showed weak crystallization ability with a weak crystallization peak (T_c) (93.3°C), a strong T_{cc} (118.4°C), and a melting endothermic peak (T_m) (165.0°C). While neat P(3HB-*co*-4HB) was soft elastomeric material with only a T_g of -8.9°C. Compared with neat PLA in Figure 5(a,b), (70/30) blend exhibited a strong sharp T_c without a T_{cc}, indicating an enhanced crystallization ability. It probably resulted from the interface between phase-separation domains where may play favourable nucleation sites due to immiscibility.[32] But with only adding of DCP, the T_c disappeared and two relatively weaker T_{cc}s and lower T_ms occurred, indicating chain branches decreased the crystallization of PLA. However, for crosslinked blends, the T_c showed up and moved to higher temperature with even sharper shape than that of 70/30 blend, so did the T_ms, demonstrating that crosslinking enhanced the crystallization of PLA. This was because that disordered short chain branches which formed during the branching and/or chain scissions reactions reduced regularity in the original linear polyester backbone of PLA and then inhibited the crystallization process. While controlled amount of crosslinks formed during the crosslinking, did not restrict the mobility of polymer chains among crosslinks to crystallize, in contrast served as nucleation sites enhanced crystallization ability of PLA at given cooling rate. It is true that branching points can also be regarded as nucleation sites to increase the nucleation process in long-chain branched PP for instance,[33] but all those short chain branches reduce local regularity and inhibit the movable polymer chains to crystallize weights more. Detailed discussions were reported in our former work.[34] Accordingly, 70/30D0.05 and 70/30D0.1 decreased the crystallization ability of PLA.

In Figure 5(c,d)， the thermal behaviour of PLA/P(3HB-*co*-4HB) (30/70) blends was in the same tendency, except for 30/70 whose T_c was too low to be detected owning to the low weight content of PLA. What was more, the crystallinitys of PLA in 30/70 blends were relatively lower than those of 70/30 blends with the same contents of crosslinking agents. This finding is related to the miscibility of the blends. The PLA and P(3HB-*co*-4HB) phases showed relatively poorer compatibility and weaker interfacial adhesion in 70/30 blends than those in 30/70 blends with the same contents of DCP and TAIC, which has been proved from DMA measurements and SEM results above. So more branched/crosslinked PLA, PLA-*g*-P(3HB-*co*-4HB) copolymers, and PLA-crosslink-P(3HB-*co*-4HB) network occurred in the 30/70 blends, reduced the PLA domains and the final crystallinity.

Figure 5

Table 1

Rheological properties

The effect of frequency on the complex viscosity $|\eta^*|$, the storage modulus G' (solid symbols), the loss modulus G'' (open symbols) and tan δ for PLA/P(3HB-*co*-4HB) blends are shown in Figure 6. It was obvious that the $|\eta^*|$ of blank 70/30 and 30/70 blend exhibited Newtonian liquid behaviour, in contrast, the $|\eta^*|$ of other blends showed non-Newtonian shear-thinning behaviour as shown in Figure 6(a,d). The $|\eta^*|$ diverged at low shear rates with high gel fractions as expected. Especially, both the $|\eta^*|$ and G' increased with the increasing of crosslinking agents. In low frequency region, both 70/30-D0.2T0.2 and 30/70-D0.2T0.2 exhibited more solid-like behaviour than those of the blank blends. This was because branching points and/or crosslinks formed a chain network that enhanced the interaction among macromolecules. However, there were exceptions for 70/30-D0.1 and 30/70-D0.1 who showed lower $|\eta^*|$ and G' values than those of 70/30-D0.05 and 30/70-D0.05 accordingly, the reason may be the competitive reactions between branching and chain scissions with active free radicals. And branching reaction was dominant over chain scissions with low adding of DCP (D0.05), while chain scissions exceeded as more free radicals initiated by higher content of DCP (D0.1). Additionally, both the $|\eta^*|$ and G' of 70/30 blends were lower than those of 30/70 blends with the same crosslinking agents contents. This was because the chain entanglement was enhanced to a higher level in 30/70 blends than that in70/30 blends. Moreover, the tan δ (tan δ =G″/G′), the ratio of energy dissipated to energy stored per cycle, was shown in Figure 6(c,f). The branched blends were predominantly viscous, tan δ >1 for the entire frequency range, and the peaks of the curves shifted to low frequency with increasing the content of DCP due to the formation of branching structure. And, the tan δ of 70/30-D0.1 was higher than that of 70/30-D0.05 because more chain scissions happened as mentioned above, so was 30/70-D0.1. Other crosslinked blends showed tan δ <1 for the entire frequency range, indicating a solid-like behaviour.

Figure 6

In Figure 7, the phase angle δ is plotted versus the absolute value of the complex modulus $|G^*|$ for PLA/P(3HB-*co*-4HB) blends. In the literature, this plot is known as the van Gurp-Palmen plot, which can be used to detect the rheological property of branched/crosslinked polymer.[17] The δs of blank 70/30 blend and 30/70 blend were close to 80° and became smaller when only adding DCP, but all indicating of a flow behaviour which was presented by a viscoelastic fluid. In contrast, the lightly crosslinked PLA/P(3HB-*co*-4HB) blends with a network structure resembled the behaviour of a fluid–solid transition with a corresponding phase angle near 45°. While 70/30-D0.2T0.2 and 30/70-D0.2T0.2 presented a phase angle of 20°, owning to heaver crosslinking and a finer compatibility and stronger interfacial adhesion among the PLA and P(3HB-*co*-4HB) phases.

Figure 7

Mechanical properties

The PLA used in this study is brittle with a low elongation at break (5%), while P(3HB-*co*-4HB) is ductile with an elongation at break of 2122% and yield strength of 5.3 MPa. The elongation at break of PLA was improved on a large scale by the incorporation with P(3HB-*co*-4HB). Typical stress-strain curves

RSC Advances Accepted Manuscript

This journal is © The Royal Society of Chemistry [year]

of PLA/P(3HB-*co*-4HB) blends are shown in Figure 8, and the detailed data of mechanical properties are listed in Table 2. Compared with other mechanical properties, the elongation at break (ε_b) is more sensitive to the compatibilization effect in immiscible binary blends. The blank 70/30 blend presented an improved ε_b of 186%. In the presence of 0.05 wt% DCP, the ε_b increased to 239%, indicating a ductile behaviour. This could be ascribed to the enhanced interfacial adhesion. With 0.1 wt% DCP, the ε_b of the blend was increased to 317%, the yield tensile strength and modulus were decreased a bit. But with the addition both DCP and TAIC, the crosslinking network formed which restricted the mobility of polymer chains to dissipate energy under tensile load. The ε_b finally decreased to 251%, while the yield tensile strength and modulus were improved slightly. Thus the tensile toughness of 70/30 blends was significantly enhanced.

The overall mechanical properties of 30/70 blends were improved as well after the in-situ compatibilization, as shown in Table 2. All the elongation at break, yield tensile strength and modulus were in the same trend with that of 70/30 blends. The elongation at break increased sharply, yield tensile strength and modulus of 30/70 blends decreased greatly duo to the incorporation of increased contents soft elastomeric component, P(3HB-*co*-4HB), as expected.

Figure 8

Table 2

To explore the fracture behaviour of PLA/P(3HB-*co*-4HB) blends in tensile tests, the morphology of fracture surfaces of the specimens was observed by SEM. Figure 10 shows SEM micrographs of tensile fractured surface and the surface parallel tensile direction near the broken point of the blends. For comparison, neat PLA, XPLA, neat P(3HB-*co*-4HB) and XP(3HB-*co*-4HB) are showed in Figure 9 (PLA and P(3HB-*co*-4HB) were crosslinked separately by both adding 0.1 wt% DCP and 0.1 wt% TAIC, the resultant samples were designated as XPLA and XP(3HB-*co*-4HB) with the gel fraction about 40%.). Neat PLA, showed fairly smooth fracture surface and typical brittle fracture, the parallel surface was flat too as showed in Figure 9(a, a′). For XPLA in Figure 9(b), the fracture surface showed a large amount of cavitations and large scale plastic deformation or fibrillation, which was related to enhanced chain entanglement caused by crosslinking network. But the parallel surface was still flat in Figure 9(b′). On the other hand, in Figure 9(c, d, c′, d′) both neat P(3HB-*co*-4HB) and XP(3HB-*co*-4HB) exhibited large scale plastic deformation without fibrous structure on the fracture surface and the parallel surface became rough. What was more, one can observe little particles in the P(3HB-*co*-4HB) matrix which was on common with other researchers.[35,36] As for blank 70/30 blend, the fracture surface changed from smooth to rough compared with that of neat PLA. There presented many little particles with clear interface and the PLA matrix started to deform with visible plastic deformation in Figure 10(a) and the parallel surface showed protuberant ridge lines and some non-uniform pores occurred in Figure 10(a′), which implied a ductile fracture behaviour. This is related to the elastic P(3HB-*co*-4HB) particles acted as stress concentrators. The consequent stress concentration leads to the development of a triaxial stress in P(3HB-*co*-4HB) particles. Because of the lack of phase adhesion, debonding can easily take place at the particle-matrix interface in the perpendicular external stress direction.[32] Thus, in Figure 10(a′) the cavities raised and were more clearly observed on the parallel surface. The fracture surface of 70/30-D0.05 was rough as well and had obvious ridges due to the plastic deformation in Figure 10(b). And P(3HB-*co*-4HB) particles seemed getting larger duo to an enhanced phase adhesion formed thicker interface layer which bedded the particles. And in Figure 10(b′) ridge lines on the parallel surface became blurred with small pores due to enhanced plasticity of PLA matrix. For 70/30-D0.1 in Figure 10(c), the fracture surface became more and more rough, which was related to easier plastic deformation of PLA chains induced by finer interface adhesion and stronger entanglement between the two polymer domains caused by branching. The ridge lines on the parallel surface turned to lots of gibbosities in Figure 10(c′). Especially for the blends with crosslinking network formed in Figure 10(d, e), the fracture surfaces showed a large amount of cavitations and large scale plastic deformation and the fibrous structure occurred, which implied a dramatic toughening effect. Moreover in Figure 10(d′, e′) the parallel surface turned flat, which was similar to that of XPLA in Figure 9(b′). The cavitations and plastic deformation induced energy dissipation and therefore led to the improvement in tensile toughness of the PLA/P(3HB-*co*-4HB) blends.[37,38]

As for five 30/70 blends in Figure 10(f-m), the particles were more apparently viewed after tensile tests than those of 70/30 blends. In Figure 10(f), the PLA particles were exposed and only P(3HB-*co*-4HB) deformed under the stretching. The parallel surface was rough with some pores on it. And then by adding DCP, the PLA particles trimmed down in Figure 10(g, h) and huge plastic fibrillation of the P(3HB-*co*-4HB) matrix was achieved. The parallel surface showed many gibbosities in Figure 10(g′, h′) with a few little pores. When the crosslinking network introduced in 30/70D0.1T0.1, it restricted the flexible P(3HB-*co*-4HB) polymer chains to deform to certain extent, the ability of plastic deformation was limited in Figure 10(l), and the parallel surface showed uniform accordion-structure perpendicularly along the tensile direction in Figure 10(l′). As for 30/70D0.2T0.2, in Figure 10(m) the plastic deformation of P(3HB-*co*-4HB) matrix was confined on a large scale, and the parallel surface displayed clear striking ridge lines. The plastic deformation of matrix and the debonding process were the two important ways induced energy dissipation and led to a toughened, biodegradable polymer blend. The conclusion is that both the compatibility between PLA component and P(3HB-*co*-4HB) component and the entanglement among polymer chains are two necessary for toughness. The important point is that fine toughness requires not only high level of adhesion between particles and matrix, but also active molecular mobility which is a crucial factor for yield stress and plastic flow.

Figure 9

Figure 10

To further investigate the toughening mechanism of PLA/P(3HB-*co*-4HB) blends, the amplified images of the strain-hardening area of stress-strain curves are show in Figure 8 for its stable increase of stress with growing strain. For comparison, neat PLA, XPLA, neat P(3HB-*co*-4HB) and XP(3HB-*co*-4HB) are showed in Figure 11. In Figure 11(a), neat PLA showed no distinct yield point with subsequent failure by neck instability,

RSC Advances Accepted Manuscript

while XPLA with a gel fraction about 40%, exhibited an enhanced yield stress and ε_b, whose stress-strain curve showed "pulse-growth" after yielding. For neat P(3HB-*co*-4HB) and XP(3HB-*co*-4HB) in Figure 11(b), they showed clear yielding and stable neck growing through cold drawing, the stress-strain curve showed "step-growth" with increasing strain, but the steps of XP(3HB-*co*-4HB) were squeezed. As for five 70/30 blends, the stress-strain curves all showed pulse-growth as strain arising, and in five 30/70 blends they became even more complicated, including both step-growth and a combination of pulse-growth and step-growth. This phenomenon was also observed in our other former work [32], unfortunately, lack of enough investigation, the mechanism behind it has been puzzled us for a long time. Here we attempted to depict the pulse-growth and step-growth as follows. As shown, the stress-strain curve of a typical ductile material owning a very long strain-hardening region, like P(3HB-*co*-4HB) used in the work, behaves step-growth. That is, as the strain growing under tensile load, the stress arises accordingly, and when the strain continues to grow, the stress will stop to a certain point and keep at that value, implying a short stress-holding behaviour during which certain amount of flexible entangled polymer chains begin to flow or orientate to dissipate energy. And then when the strain keeps on growing, another new short stress-holding process happens with higher stress value. The apparent phenomenon is the stable growing of the neck region from its two ends. In contrast, the stiff and brittle polymer, like PLA, shows no distinct yield point before its failure. After proper crosslinking or toughened by adding small amount of another soft material, like P(3HB-*co*-4HB), the stress-strain curve of brittle polymer will present pulse-growth. That is, as the strain growing under the tensile load, the stress increases to a point and suddenly drops a bit with the continuing growing of strain because there are only limited numbers of rigid polymer chains (compared with P(3HB-*co*-4HB) chains) to orientate. It is just those continuous newly emerging rigid polymer chains with very limit degree of orientation that to dissipate energy during the neck growing process. So when the strain keeps on growing, another new pulse-growth happens. But the apparent phenomenon is the same growing of a neck region. Compared with the pulse-growth, in order to hold that stress, it needs larger number of flexible polymer chains to orientate in the step-growth. As described by other researchers[39], in reality, the fracture mechanisms of polymeric materials are the combination of chain scission and slippage (pull-out) which is governed by entanglements and polymer molecular weight. Therefore an enhanced entanglement of polymer chains by introducing proper amount of crosslinks in XPLA can restrict the chain scission or slippage to some extent, thus giving opportunities for small amount of polymer chains to flow, compared with only rigid PLA chains with limited physical entanglement. And since there is only 30% flexible polymer chains of P(3HB-*co*-4HB) in 70/30 blends, the stress-strain curves of crosslinked XPLA and 70/30 blends all showed pulse-growth due to relatively rigid polymer chains. Meanwhile for 30/70 blends, they included both step-growth with flexible entangled polymer chains, and a combination of pulse-growth and step-growth with decreased flexibility of polymer chains. Furthermore, we can infer that for those polymer chains which are not only very flexible but also entangled together with proper amount, like rubber, the stress-strain curves will grow smoothly due to the easy flow of polymer chains in response to applied stress. Sometimes, one can introduce proper amount of chemical entanglement to enhance the weak and low degree of limited physical entanglement.

Additionally, the detailed average $\Delta\sigma$ and $\Delta\varepsilon$ values are listed in Table 3 (In step growth, the $\Delta\sigma$ is the difference of two stress values between two steps; and in pulse increase, the $\Delta\sigma$ is the difference of peak stress value minus the following valley one. All the $\Delta\varepsilon$ values are calculated according to the $\Delta\sigma$.). In 70/30 blends, the $\Delta\varepsilon$ values of 70/30 and 70/30-D0.2T0.2 were a bit smaller than those of other three 70/30 blends and XPLA due to poorer compatibility between two polymer components and heavier crosslinking. And the $\Delta\sigma$ values of the blends were all lower than that of XPLA because of the introduce of soft P(3HB-*co*-4HB). In addition, for 30/70 blends, the $\Delta\varepsilon$ values of all detected blends and XP(3HB-*co*-4HB) were near 2%, which much lower than that of neat P(3HB-*co*-4HB) (11.6%) owning to limited mobility of polymer chains. For four enhanced compatibility 30/70 blends, the entanglement among polymer chains was increased compared with blank 30/70 blend, so the $\Delta\sigma$ values increased a little finally. Consequently, it is both the flexibility of polymer chain itself and the degree of chain entanglement and their cooperation that vary stress-strain curves.

Figure 11

Table 3

Conclusions

Highly enhanced compatibilization of biosourced and biodegradable PLA and P(3HB-*co*-4HB) blends were prepared by reactive melt compounding. The miscibility, phase morphology, thermal behaviour, rheological and mechanical properties of the blends were investigated by DMA, SEM, DSC and tensile tests in detail. DMA and SEM results indicated that the miscibility of two immiscible components was enhanced to different extents due to the different introduces of branching and crosslinking. And larger shifts toward each other of T_gs, a larger reduction of dispersed phase particle size and more significant increase of the interfacial adhesion of the PLA and P(3HB-*co*-4HB) were achieved after crosslinking than that of branching and blank blends. And the branches decreased the crystallization ability of PLA, while crosslinking enhanced it on a large scale. Moreover, the blends exhibited remarkable improvement of rheological properties in the melt state when compared with that of blank PLA/P(3HB-*co*-4HB) blends. The transition from the liquid-like to the solid-like viscoelastic behaviours at low frequencies demonstrated that the formation of crosslinking network. With increasing the content of DCP, the blends showed increased yield tensile strength, modulus, and elongation at break. However as DCP cooperated with TAIC, the elongation at break decreased because of crosslinking network limited the mobility of polymer chains. The magnified images of strain-hardening of the stress-strain curves for the blends showed step-growth with flexible entangled polymer chains and pulse-growth with rigid polymer chains. Furthermore, SEM images of the fracture surfaces of the blends after tensile tests presented the fracture behaviour changed from brittle fracture behaviour for neat PLA to ductile fracture

RSC Advances Accepted Manuscript

This journal is © The Royal Society of Chemistry [year]

behaviour for the blends. The plastic deformation of matrix and the debonding process were the two important ways induced energy dissipation and led to a toughened blend. The important point is that fine toughness requires not only high level of adhesion between particles and matrix, but also enough molecular mobility which is a crucial factor for yield stress and plastic flow.

Acknowledgement

The authors are grateful for financial support from the National Science Foundation of China (51021003).

Notes and references

[a] *Key Laboratory of Polymer Ecomaterials, Changchun Institute of Applied Chemistry, Chinese Academy of Sciences, 5625 Renmin Street, Changchun 130022, People's Republic of China; Tel: 86-0431-85262890; E-mail: dongls@ciac.ac.cn*

[b] *University of Chinese Academy of Sciences, No. 19A Yuquanlu, Beijing 100049, People's Republic of China*

1. Cassagnau, P.; Michel, A. *Polymer* **2001**, *42*, 3139-3152.
2. Jiang, L.; Michael, P.W.; Zhang, J.W. *Biomacromolecules* **2006**, *7*, 199-207.
3. Taguet, A.; Huneault, M.A.; Favis, B.D. *Polymer* **2009**, *50*, 5733-5743.
4. Chen, X.H.; Ma, G.Q.; Li, J.Q.; Jiang, S.H.; Yuan, X.B.; Sheng, J. *Polymer* **2009**, *50*, 3347-3360.
5. Díaz, M.F.; Barbosa, S.E.; Capiati, N.J. *Polymer* **2007**, *48*, 1058-1065.
6. Wang, X.M.; Zhuang, Y.G.; Dong, L.S. *J Appl Polym Sci* **2012**, *126*, 1876-1884.
7. Ou, B.L.; Li, D.X. *Polym Bull* **2009**, *63*, 441-447.
8. Abe, H.; Doi Y.; Kumagai, Y. *Macromolecules*, **1994**, *27*, 6012-6017.
9. Li, W.J.; József, K.K.; Alois, K.; Schlarb. *Macromol Mater Eng* **2009**, *294*, 582-589.
10. Kwak, S.Y.; Nakajima, N. *Macromolecules*, **1996**, *29*, 5446-5452.
11. Elias, L.; Fenouillot, F.; Majeste, J.C. *Polymer* **2007**, *48*, 6029-6040.
12. Elias, L.; Fenouillot, F.; Majeste, J.C.; Cassagnau, P. *Polymer* **2008**, *49*, 4378-4385.
13. Hong, J.S.; Han, N.K.; Ahn, K.H.; Lee, S.J.; Kim, C. *Polymer* **2006**, *47*, 3967-3975.
14. Kim, J.K.; Jang, J.; Lee, D.H.; Ryu, D.Y. *Macromolecules*, **2004**, *37*, 8599-8605.
15. Hong, J.S.; Kim, Y.K.; Ahn, K.H.; Lee, S.J.; Kim, C. *Rheol Acta* **2007**, *46*, 469-478.
16. Zlata, H.M.; Želimir, J.; Vera, K.; Marica, M.M.; Jasenka, J. *Macromol Mater Eng* **2002**, *287*, 684-692.
17. Wu, D.F.; Zhang, Y.S.; Zhang, Yu. W. *Biomacromolecules* **2009**, *10*, 417-424.
18. Sun, S.L.; Xu, X.Y.; Yang, H.D.; Zhang, H.X. *Polymer* **2005**, *46*, 7632-7643.
19. Yoon, J.S.; Lee, W.S.; Kim, K.S.; Chin, I.J.; Kim, M.N.; Kim, C. *Eur Polym J* **2000**, *36*, 435-442.
20. Semba, T.; Kitagawa, K.; Ishiaku, U.S.; Hamada, H. *J Appl Polym Sci* **2006**, *101*, 1816-1825.
21. Semba, T.; Kitagawa, K.; Ishiaku, U.S.; Kotaki, M.; Hamada, H. *J Appl Polym Sci* **2007**, *103*, 1066-1074.
22. Wang, R.Y.; Wang, S.F.; Zhang, Y.; Wan, C.Y.; Ma, P.M. *Polym Eng Sci* **2009**, *49*, 26-33.
23. Saito, Y.; Nakamura, S.; Hiramitsu, M.; Doi, Y. *Polym Int* **1996**, *39*, 169-174.
24. Ishida, K.; Wang, Y.; Inoue, Y. *Biomacromolecules* **2001**, *2*, 1285-1293.
25. Doi, Y.; Kunioka, M.; Nakamura, Y.; Soga, K. *Macromolecules* **1988**, *21*, 2722-2727.
26. Mitomo, H.; Hsieh, W.C.; Nishiwaki, K.; Kasuya, K.; Doi, Y. *Polymer* **2001**, *42*, 3455-3461.
27. Lee, W.H.; Mohd, N.M.; Azizan; Kumar, S. *Polym Degrad Stab* **2004**, *84*, 129-134.
28. Matsumoto, A. *Prog Polym Sci* **2001**, *26*, 189-257.
29. Mitomo, H.; Kaneda, A.; Quynh, T.M.; Nagasawa, N.; Yoshii, F. *Polymer* **2005**, *46*, 4695-4703.
30. Han, L.J.; Han, C.Y.; Zhang, H.L.; Chen, S.; Dong, L.S. *Polym Compos* **2012**, *33*, 850-859,
31. Liu, L.J.; Li, S.M.; Garreau, H.; Vert, M. *Biomacromolecules* **2000**, *1*, 350-359.
32. Wang, X.M.; Zhuang, Y.G.; Dong, L. *J Appl Polym Sci* **2012**, *127*, 471-477.
33. Wan, D.; Zhang, Z.; Wang, Y.; Xing, H; Jiang, Z. Tang, T. *Soft Matter* 2011, 7, 5290-5299.
34. Bian, Y.; Han L.; Han, C.; Lin, H.; Zhang, H.; Bian, J. Dong, L. *CrystEngComm* 2014, 16, 2702-2714.
35. Han, H.Y.; Wang, X.D.; Wu, D.C. *Ind Eng Chem Res* **2012**, *51*, 14047-14060.
36. Zhang, R.; Zhu, C.J.; Shan, X.Y.; Xia, J.; Zhu, Q.; Hu, Y. *J Appl Polym Sci* **2013**, *130*, 2015-2022
37. Jiang, L.; Wolcott, M.P.; Zhang, J.W. *Biomacromolecules* **2006**, *7*, 199-207.
38. Li, Y.J.; Shimizu, H. *Macromol Biosci* **2007**, *7*, 921-928.
39. Sperling, L.H. In *Introduction to physical polymer science*, 4th ed.; John Wiley & Sons, Inc.; Wiley-Interscience: New Jersey, 2006; p 557-612.

RSC Advances Accepted Manuscript

Figure captions:

Figure 1. Gel fraction of PLA, P(3HB-*co*-4HB), and PLA/P(3HB-*co*-4HB) blends.

Figure 2. DMA traces of PLA/P(3HB-*co*-4HB) blends, tanδ versus temperature of (a)70/30blends, (b) 30/70 blends. The *E'* versus temperature of (c) 70/30blends, (d) 30/70 blends (the insets give details of the transitions).

Figure 3. SEM micrographs of cryo-fractured surfaces of PLA/P(3HB-*co*-4HB) blends after selective enzymatic removal of dispersed phase domains, (a) 70/30, (b) 70/30-D0.05, (c) 70/30-D0.1, (d) 70/30-D0.1T0.1, (e) 70/30-D0.2T0.2, (f) 30/70, (g) 30/70-D0.05, (h) 30/70-D0.1, (l) 30/70-D0.1T0.1, (m) 30/70-D0.2T0.2.

Figure 4. Plots of complex viscosity $|\eta^*|$ versus frequency.

Figure 5. DSC curves of PLA/P(3HB-*co*-4HB) blends, (a) first cooling of 70/30 blends, (b) second heating of 70/30 blends, (c) first cooling of 30/70 blends and (d) second heating of 30/70 blends.

Figure 6. Plots of (a) complex viscosity |η*|, (b) storage modulus G' (solid) and loss modulus G" (open) and (c) tan(δ) versus frequency of 70/30 blends. Plots of (d) complex viscosity |η*|, (e) torage modulus G' (solid) and loss modulus G" (open) and (f) tan(δ) versus frequency of 30/70 blends.

Figure 7. van Gurp-Palmen plots of phase angle (δ) versus complex modulus (|G*|) of (a) 70/30 blends and (b) 30/70 blends.

Figure 8. Tensile stress-strain curves of (a) 70/30 blends and (b) 30/70 blends.

Figure 9. (a) Schematic diagram of the measurement locations B, fractured surface, and C, surface parallel tensile direction near the broken points and the SEM of PLA/P(3HB-*co*-4HB) blends in tensile tests, (b, b') PLA, (c, c') XPLA, (d, d') P(3HB-*co*-4HB) and (e, e') XP(3HB-*co*-4HB) in tensile tests. (b-e, fractured surface, b'-e', surface parallel tensile direction near the broken points)

Figure 10. SEM micrographs of PLA/P(3HB-*co*-4HB) blends during tensile tests, (a-m, fractured surface, a'-m', surface parallel tensile direction near the broken points), (a, a') 70/30, (b, b') 70/30-D0.05, (c, c') 70/30-D0.1, (d, d') 70/30-D0.1T0.1, (e, e') 70/30-D0.2T0.2, (f, f') 30/70, (g, g') 30/70-D0.05, (h, h') 30/70-D0.1, (l, l') 30/70-D0.1T0.1 and (m, m') 30/70-D0.2T0.2.

Figure 11. Tensile stress-strain curves of (a) PLA and XPLA, (b) P(3HB-*co*-4HB) and XP(3HB-*co*-4HB).

RSC Advances Accepted Manuscript

This journal is © The Royal Society of Chemistry [year]

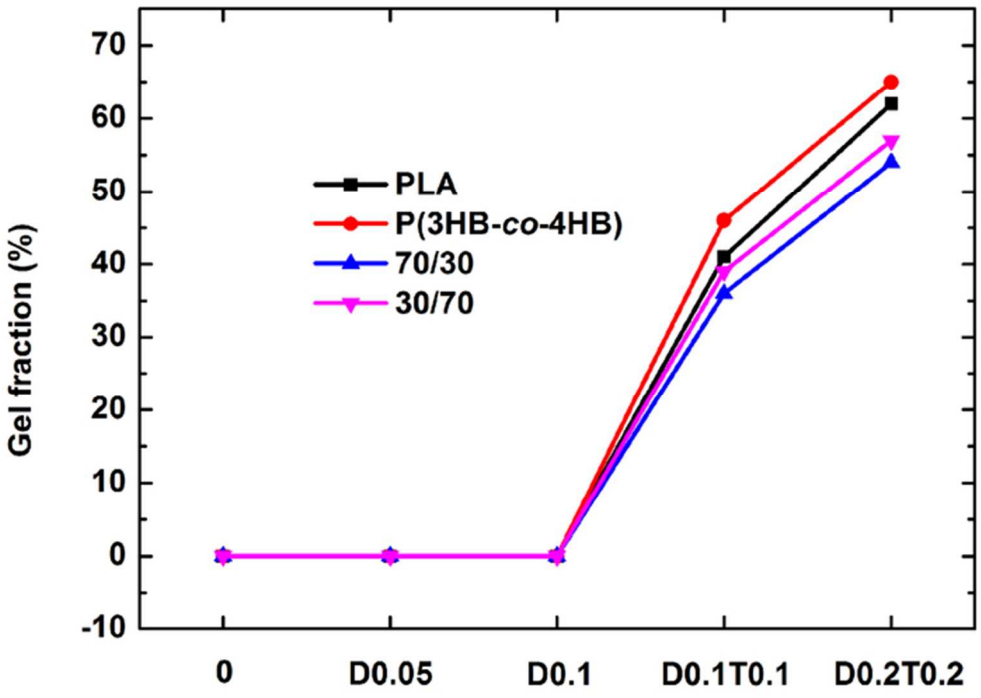

60x43mm (300 x 300 DPI)

RSC Advances Accepted Manuscript

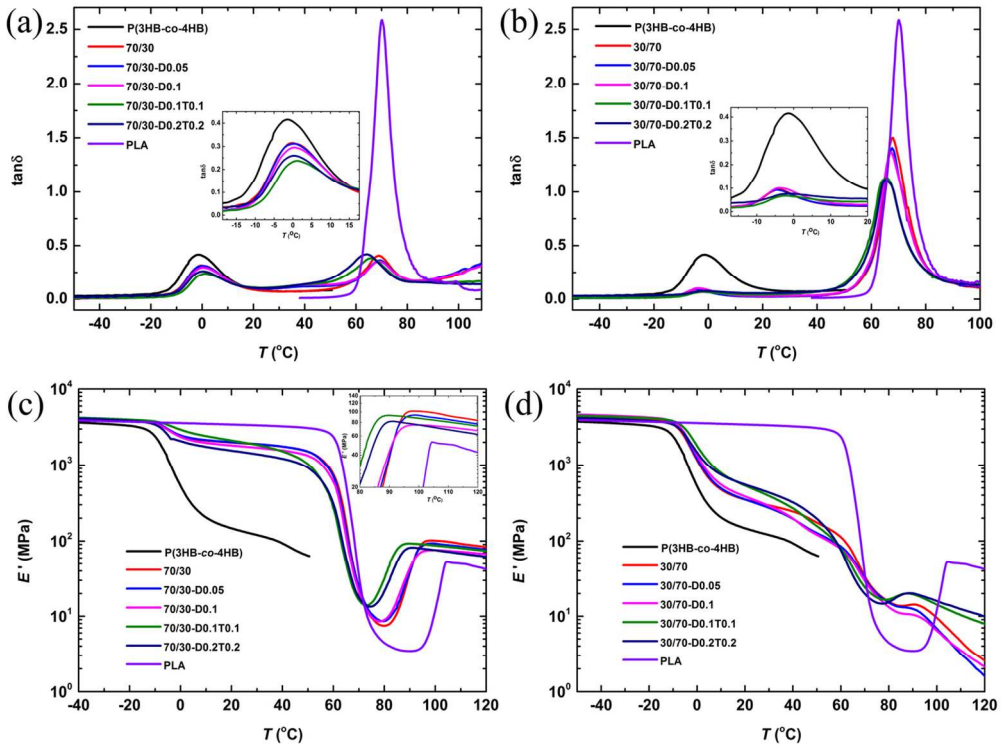

128x97mm (300 x 300 DPI)

RSC Advances Accepted Manuscript

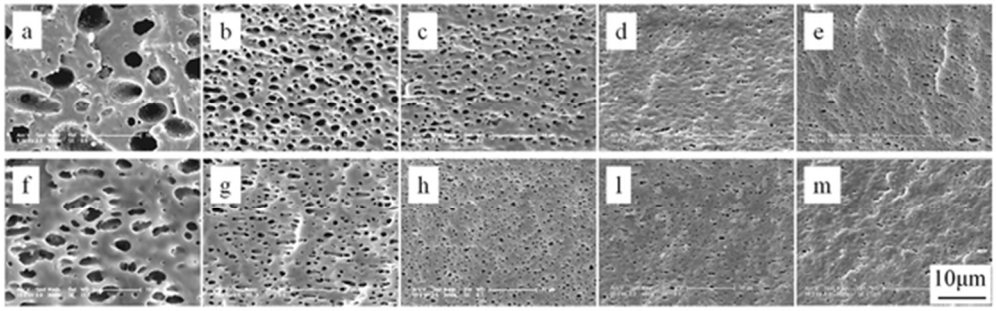

53x16mm (300 x 300 DPI)

RSC Advances Accepted Manuscript

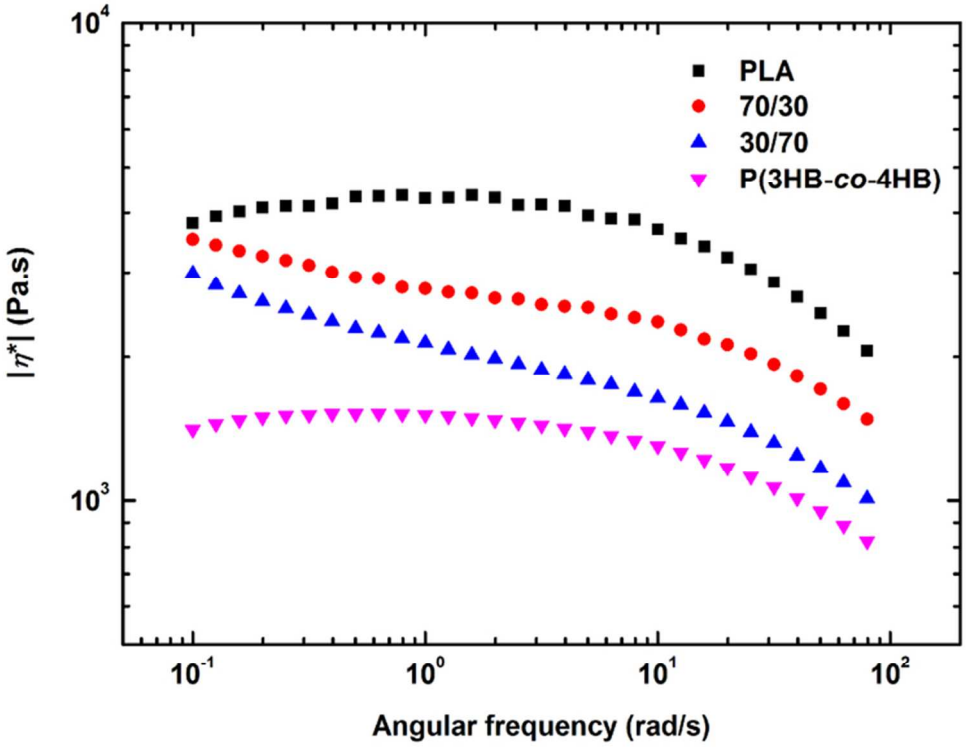

65x50mm (300 x 300 DPI)

RSC Advances Accepted Manuscript

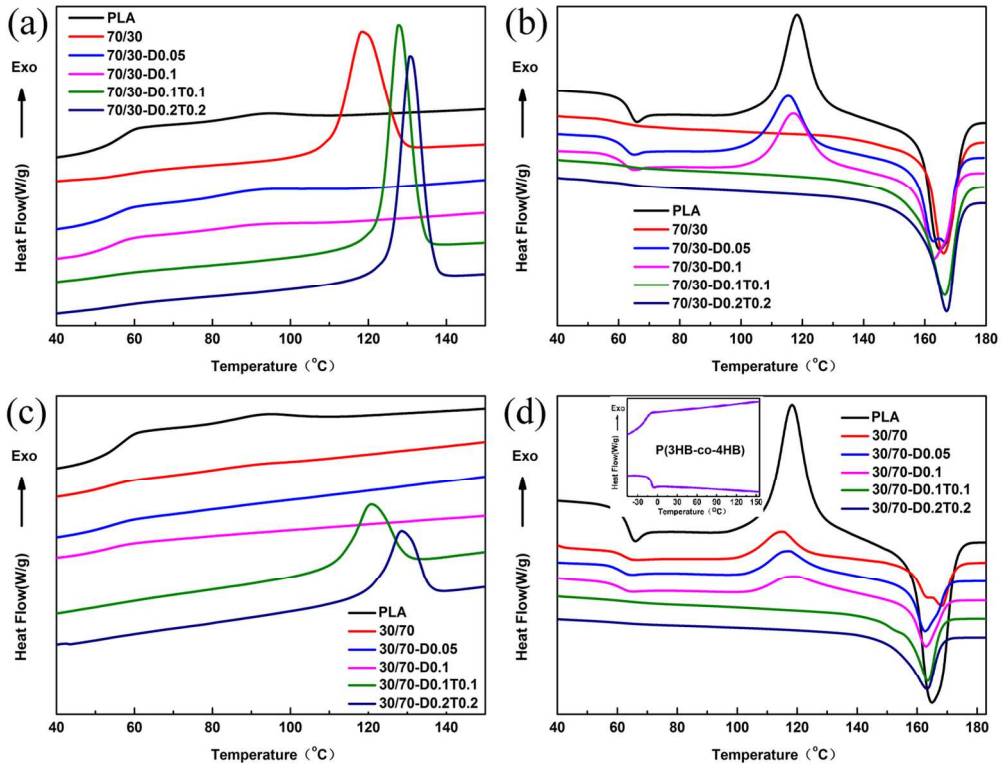

132x102mm (300 x 300 DPI)

RSC Advances Accepted Manuscript

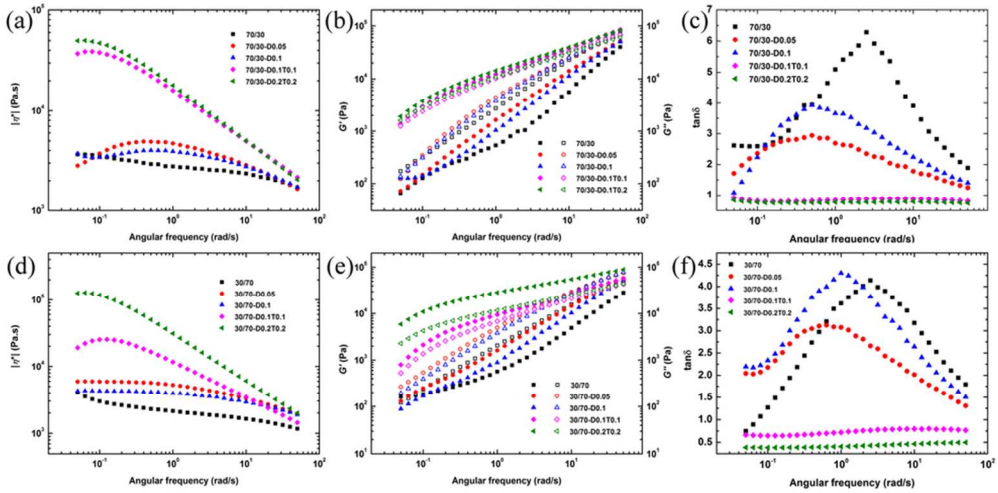

83x41mm (300 x 300 DPI)

RSC Advances Accepted Manuscript

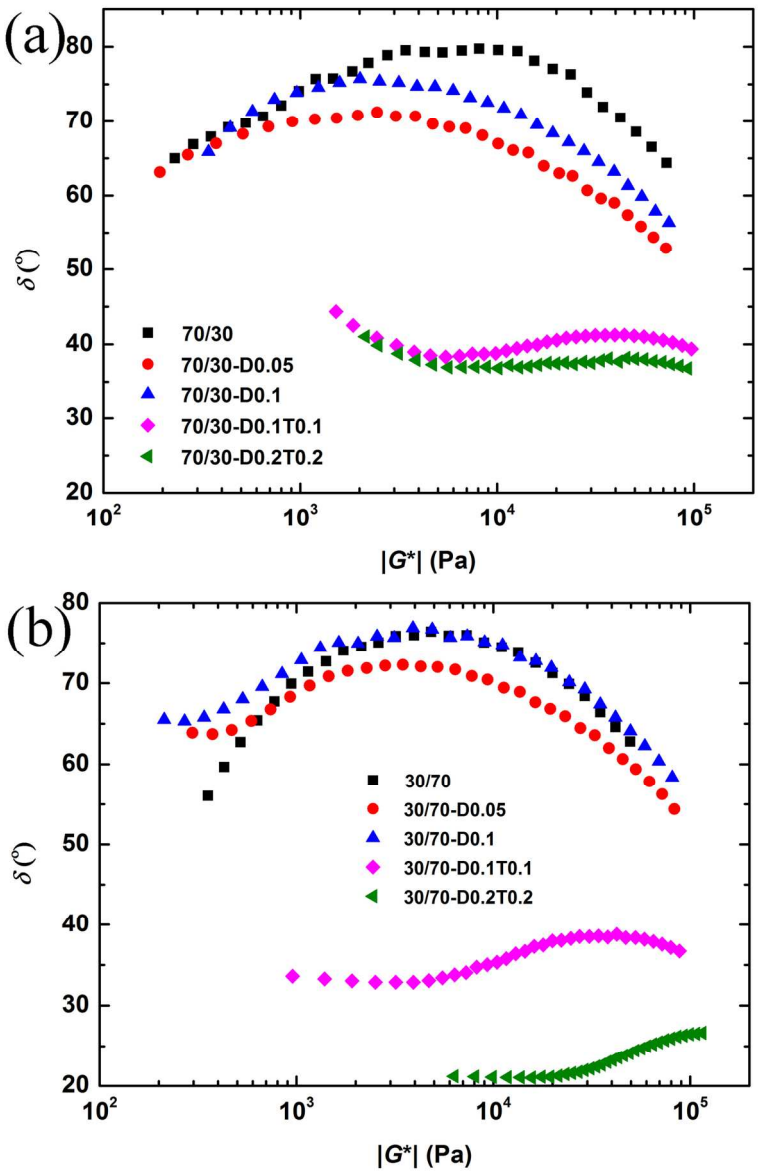

132x205mm (300 x 300 DPI)

RSC Advances Accepted Manuscript

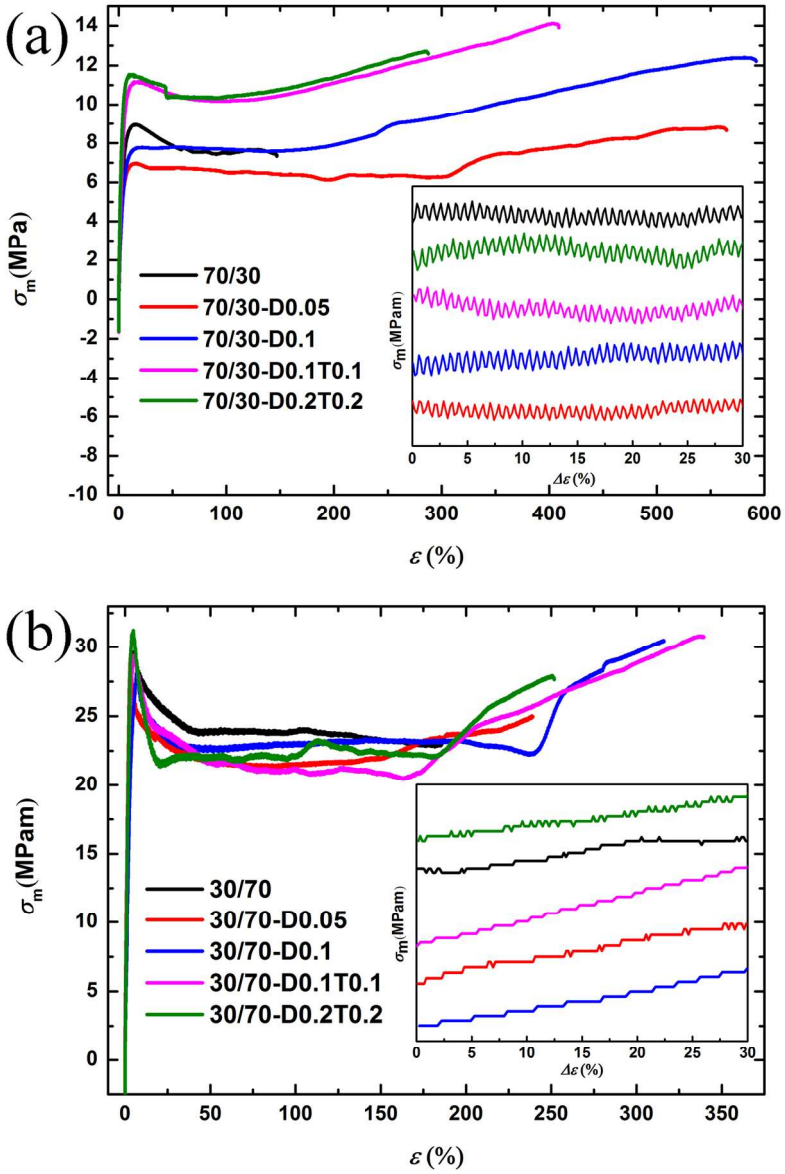

128x195mm (300 x 300 DPI)

RSC Advances Accepted Manuscript

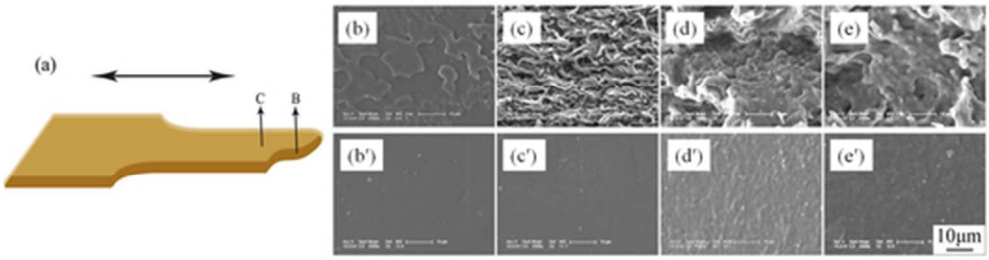

45x12mm (300 x 300 DPI)

RSC Advances Accepted Manuscript

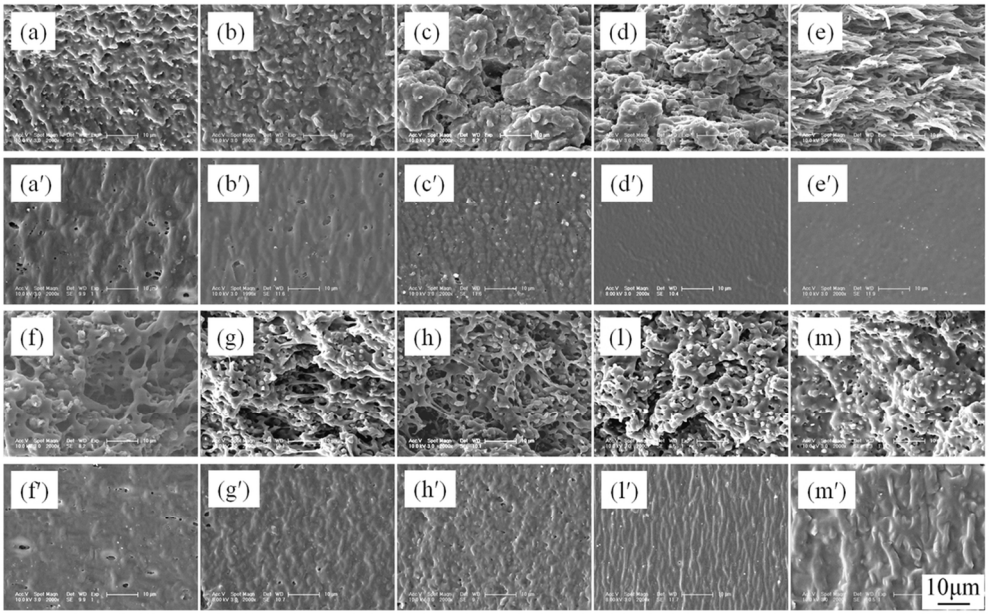

106x66mm (300 x 300 DPI)

RSC Advances Accepted Manuscript

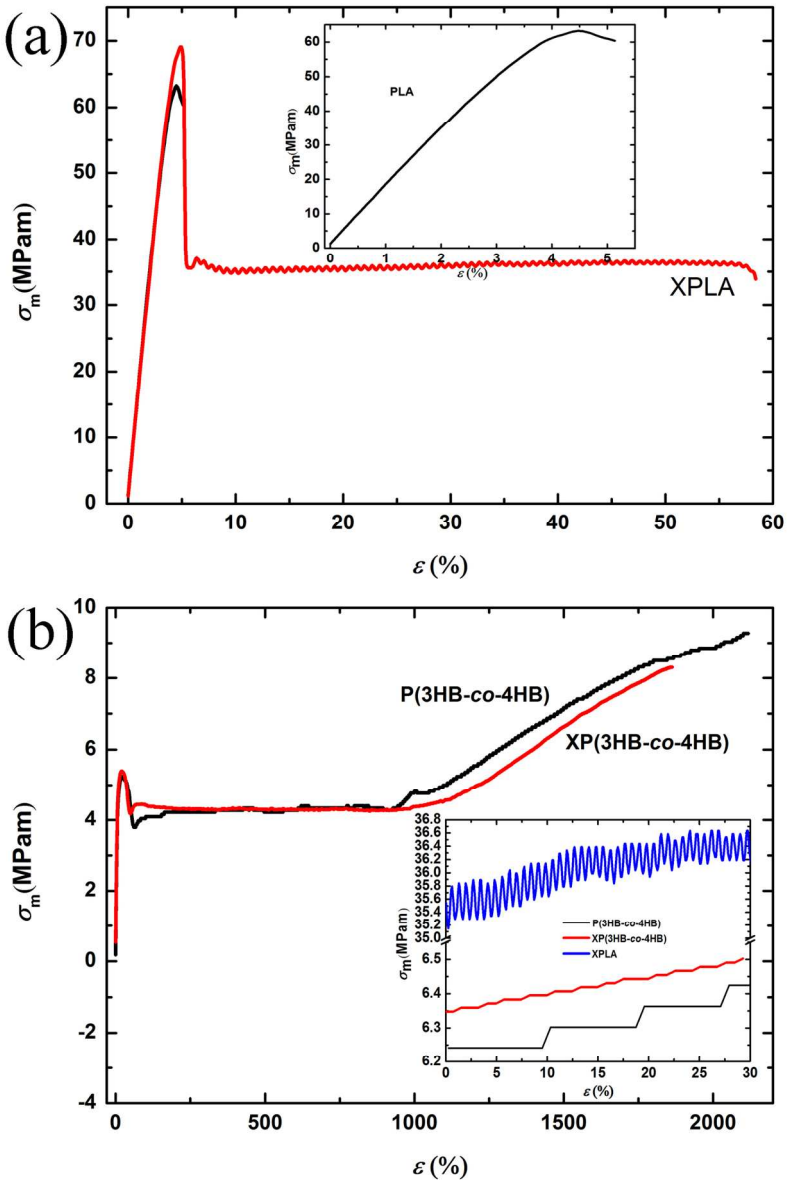

128x193mm (300 x 300 DPI)

RSC Advances Accepted Manuscript

Table 1. Thermal and crystalline properties of PLA/P(3HB-*co*-4HB) blends

Sample	DMA			DSC								
	$T_{g,P(3HB\text{-}co\text{-}4HB)}$ (°C)	$T_{g,PLA}$ (°C)	ΔT_g (°C)	T_g (°C)	T_{cc} (°C)	ΔH_{cc}[a] (J/g)	T_c (°C)	ΔH_c[a] (J/g)	T_{m1} (°C)	T_{m2} (°C)	ΔH_m[a] (J/g)	X_c[b] (%)
PLA	-	70.2	-	63.9	118.4	34.6	93.3	2.3	-	165.0	36.6	39.4
70/30	-3.5	67.6	71.1	59.4	-	-	118.4	37.6	-	166.1	43.6	46.9
70/30-D0.05	-3.5	67.5	71.0	62.5	116.4	32.4	-	-	162.7	166.6	38.0	40.9
70/30-D0.1	-3.4	67.1	70.5	62.4	118.2	31.1	-	-	163.1	-	34.8	37.4
70/30-D0.1T0.1	-1.1	65.4	66.5	62.7	-	-	131.2	44	-	165.5	48.8	52.5
70/30-D0.2T0.2	-0.9	65.2	66.1	63.5	-	-	130.9	42.8	-	165.9	47.7	51.3
30/70	0.1	68.9	68.8	61.9	114.9	28.3	-	-	164.3	168.1	37.0	39.8
30/70-D0.05	0.1	69.0	68.9	61.9	117.2	26.3	-	-	162.7	-	35.7	37.5
30/70-D0.1	0.5	69.0	68.5	61.4	118.8	24.7	-	-	162.9	-	31.3	33.6
30/70-D0.1T0.1	0.9	65.7	64.6	62.1	-	-	120.7	35.3	163.6	-	44.3	47.6
30/70-D0.2T0.2	0.8	64.1	63.3	-	-	-	128.5	34	163.3	-	42.0	45.2
P(3HB-*co*-4HB)	-1.6	-	-	-	-	-	-	-	-	-	-	

[a] ΔH_{cc} and ΔH_m are corrected for the content of PLA in the blend.

[b] Degree of crystallinity, calculated from the ratio of ΔH_m[a] and ΔH_m^0 (the melting enthalpy ΔH_m^0 of 100% crystalline PLA taken as 93 J/g).

Table 2. Mechanical properties of PLA/P(3HB-*co*-4HB) blends.

Sample	Yield tensile strength (MPa)	Modulus (MPa)	Elongation at break (%)	Sample	Yield tensile strength (MPa)	Modulus (MPa)	Elongation at break (%)
PLA	63.4±0.5	1985±17	5±1	P(3HB-*co*-4HB)	5.3±1.9	85±25	2122±30
XPLA	69.4±0.6	1990±20	58±23	XP(3HB-*co*-4HB)	5.6±1.1	92±21	1863±33
70/30	29.6±0.3	1227±19	186±21	30/70	14.5±0.4	239±12	145±25
70/30-D0.05	29.2±0.2	785±17	239±25	30/70-D0.05	7.0±0.3	204±15	564±30
70/30-D0.1	28.2±0.3	801±13	317±19	30/70-D0.1	7.8±0.2	174±10	593±22
70/30-D0.1T0.1	29.3±0.3	999±16	310±28	30/70-D0.1T0.1	11.0±0.2	297±14	410±28
70/30-D0.2T0.2	31.2±0.2	1123±15	251±24	30/70-D0.2T0.2	11.6±0.3	338±13	289±31

RSC Advances Accepted Manuscript

Table 3. The average $\Delta\sigma$ and $\Delta\varepsilon$ values of PLA/P(3HB-*co*-4HB) blends.

Sample	$\Delta\varepsilon$(%)	$\Delta\sigma$(MPa)	Sample	$\Delta\varepsilon$(%)	$\Delta\sigma$(MPa)
PLA	-	-	P(3HB-*co*-4HB)	11.645±2.012	0.060±0.013
XPLA	0.713±0.011	0.571±0.036	XP(3HB-*co*-4HB)	2.263±0.057	0.013±0.005
70/30	0.710±0.012	0.224±0.032	30/70	-	0.022±0.006
70/30-D0.05	0.714±0.010	0.179±0.030	30/70-D0.05	-	0.024±0.005
70/30-D0.1	0.714±0.009	0.252±0.026	30/70-D0.1	2.343±0.077	0.026±0.007
70/30-D0.1T0.1	0.713±0.013	0.187±0.023	30/70-D0.1T0.1	2.770±0.065	0.023±0.005
70/30-D0.2T0.2	0.710±0.010	0.233±0.025	30/70-D0.2T0.2	-	0.023±0.007

RSC Advances Accepted Manuscript